New Molecular Assemblies of Redox Isomers, $[Cr^{III}(X_4SQ)_{3-n}(X_4Cat)_n]^{-n}$ (X = Cl and Br; *n* = 0, 1, and 2), with Metallocenium Cations, $[M^{III}Cp_2]^+$ (M = Co and Fe): X-ray Crystal Structures and Physical Properties

Ho-Chol Chang, Hitoshi Miyasaka, and Susumu Kitagawa*

Department of Synthetic Chemistry and Biological Chemistry, Graduate School of Engineering, Kyoto University, Sakyo-ku, Kyoto 606-8501, Japan

Received April 13, 2000

A series of redox isomers of $[Cr^{III}(X_4SQ)(X_4Cat)_2]^{2-}$, $[Cr^{III}(X_4SQ)_2(X_4Cat)]^-$, and $[Cr^{III}(X_4SQ)_3]^0$ (X = Cl and Br, SQ = semiquinonate, and Cat = catecholate) have been synthesized and characterized as charge-transfer (CT) compounds with metallocenium cations: $(Co^{III}Cp_2)_2[Cr^{III}(Cl_4SQ)(Cl_4Cat)_2]$ (**1**), $(Co^{III}Cp_2)_2[Cr^{III}(Br_4SQ)(Br_4Cat)_2]$ (**2**), $(Fe^{III}Cp_2)[Cr^{III}(Cl_4SQ)_2(Cl_4Cat)]\cdot C_6H_6$ (**4**), $(Fe^{III}Cp_2)[Cr^{III}(Br_4SQ)_2(Br_4Cat)]\cdot CS_2$ (**5**), and $(Fe^{III}Cp_2)[Cr^{III}(Cl_4SQ)_2(Cl_4Cat)][Cr^{III}(Cl_4SQ)_3]$ (**6**). First, the oxidation states of the chromium complexes are strongly dependent on the redox potentials of the metallocenes used. The $Co^{II}Cp_2$, exhibiting stronger reduction power than $Fe^{II}Cp_2$, is useful for two-electron reduction of the $[Cr^{III}(X_4SQ)_3]^0$, affording $[Cr^{III}(X_4SQ)(X_4Cat)_2]^{2-}$ (**1** and **2**), which are first isolated and crystallographically characterized in the solid state. In contrast the reaction with $Fe^{II}Cp_2$ affords only $[Cr^{III}(X_4SQ)_2(X_4Cat)]^-$ (**4** and **5**). Second, solvents influence crystal structures of these compounds. The solvent set of C_6H_6/CS_2 gives 1:1:C_6H_6 compound **4** with unique charged anions, $[Cr^{III}(Cl_4SQ)_2(Cl_4Cat)]^-$, while the other set, *n*-C_6H_{12}/CS_2, affords 1:2 compound **6** including the two redox isomers, $[Cr^{III}(Cl_4SQ)_2(Cl_4Cat)]^-$ and $[Cr^{III}(Cl_4SQ)_3]^0$. The $[Cr^{III}(X_4SQ)(X_4Cat)_2]^{2-}$ anions in **1** and **2** show no significant interconnection between them (discrete type), while the $[Cr^{III}(X_4SQ)_2(X_4Cat)]^-$ anions in **4**−**6** show one-dimensional column-type structures with the aid of intermolecular stacking interactions of the ligand moieties. The anions in **4** show additional stacking interaction with the $[Fe^{III}Cp_2]^+$ to form one-dimensional ···[D][A][S][D][A]··· (D = $[Fe^{III}Cp_2]^+$, A = $[Cr^{III}(Cl_4SQ)_2(Cl_4Cat)]^-$, and S = C_6H_6) type mixed-stack arrangements similar to that of previously reported $(Co^{III}Cp_2)[Cr^{III}(Cl_4SQ)_2(Cl_4Cat)]\cdot C_6H_6$ (**3**). Compound **6** forms a two-dimensional sheet structure where the two redox isomers, $[Cr^{III}(Cl_4SQ)_2(Cl_4Cat)]^-$ and $[Cr^{III}(Cl_4SQ)_3]^0$, are included. The sheet is regarded as a mixed-valence molecular assembly. Two types of the anions, $[Cr^{III}(X_4SQ)(X_4Cat)_2]^{2-}$ (**1** and **2**) and $[Cr^{III}(X_4SQ)_2(X_4Cat)]^-$ (**4**−**6**), exhibiting an *intramolecular* mixed-valence state, show intramolecular intervalence CT transition (IVCT) from the Cat to the SQ at near 5800 and 4300 cm^{-1}, respectively, both in the solution and in the solid states. The *intermolecular* mixed-valence state of **6** was characterized by absorption spectroscopy, electric conductivity, and SQUID magnetometry. Interestingly, this mixed-valence state of the chromium module is dependent on the redox active nature of the coordinated ligands.

Introduction

Transition metal complexes with *o*-dioxolene ligands have been one of intriguing subjects of intensive research in the last few decades due to the rich redox chemistry based on a variety of formal oxidation states not only for the metal center but also for the ligand moieties.[1] Valence tautomerism involving *o*-dioxolene ligands and transition metals has been discovered and increasingly studied in recent years, especially for heteroleptic cobalt and manganese complexes, $M^{III}(SQ)(Cat)(N\text{-}N)$ (SQ = semiquinonate, Cat = catecholate, N-N = nitrogen donor).[2]

Our interest is focused on homoleptic complexes where redox isomers, SQ and Cat, are simultaneously coordinated to the metal ion to give a complex generally written as $[M(SQ)_m(Cat)_n]$ because the mixed-charge ligands are related, in a sense, to a class of complexes with mixed-valence metal ions linked by a bridging ligand. In addition, such complexes are also noted as a new type of module for molecular assemblies because in the solid phase an intermolecular SQ···SQ radical type and/or SQ···Cat charge-transfer (CT) type interactions should be expected. Several extended arrays of the *o*-dioxolene metal complexes have been found,[3] where the direct stack between the ligand moieties occurs between the adjacent complexes. The physical properties ascribed to the assembly, however, have not been reported, while the reduced and oxidized forms of metal-free *p*-benzoquinones (BQ) molecules are well-known for their ability to form stacking structures and to give conductive donor−acceptor compounds.[4] The properties arising from the coexistence of the intra- and/or intermolecular charge-transfer

(1) (a) Pierpont, C. G.; Lange, C. W. *Prog. Inorg. Chem.* **1994**, *41*, 331. (b) Pierpont, C. G.; Buchanan, R. M. *Coord. Chem. Rev.* **1981**, *38*, 45.

(2) (a) Adams, D. M.; Hendrickson, D. N. *J. Am. Chem. Soc.* **1996**, *118*, 11515. (b) Adams, D. M.; Noodleman, L.; Hendrickson, D. N. *Inorg. Chem.* **1997**, *36*, 3966. (c) Jung, O.-S.; Pierpont, C. G. *J. Am. Chem. Soc.* **1994**, *116*, 2229.

(3) (a) Pierpont, C. G.; Buchanan, R. M. *J. Am. Chem. Soc.* **1975**, *97*, 6450. (b) Buchanan, R. M.; Kessel, S. L.; Downs, H. H.; Pierpont, C. G.; Hendrickson, D. N.Pierpont, C. G.; Buchanan, R. M. *J. Am. Chem. Soc.* **1978**, *100*, 7894. (c) Pierpont, C. G.; Buchanan, R. M. *J. Am. Chem. Soc.* **1975**, *97*, 4912. (d) Speier, G.; Tisza, S.; Rockenbauer, A.; Boone, S. R.; Pierpont, C. G. *Inorg. Chem.* **1992**, *31*, 1017. (e) Pierpont, C. G.; Downs, H. H. *J. Am. Chem. Soc.* **1976**, *98*, 4834. (f) Simpson, C. L.; Pierpont, C. G. *Inorg. Chem.* **1992**, *31*, 4308.

10.1021/ic0003832 CCC: $20.00
Published on Web 12/07/2000

Scheme 1

$$Cr^{III}(X_4SQ)_3 \rightleftharpoons [Cr^{III}(X_4SQ)_2(X_4Cat)]^- \rightleftharpoons [Cr^{III}(X_4SQ)(X_4Cat)_2]^{2-} \rightleftharpoons [Cr^{III}(X_4Cat)_3]^{3-}$$

(X = Cl and Br)

interactions and local spins on the metal ions are an intriguing target when the transition metal complexes are utilized.

We present a detailed discussion about the structural features of CT compounds derived from tris(*o*-tetrahalogenosemiquinonate) chromium(III), $Cr^{III}(X_4SQ)_3$ (X = Cl and Br), which undergo electrochemical reduction at 0.82 (Cl) and 0.44 (Cl), and 0.83 (Br) and 0.43 (Br) V (vs SCE), respectively, to afford $[Cr^{III}(X_4SQ)_2(X_4Cat)]^-$ and $[Cr^{III}(X_4SQ)(X_4Cat)_2]^{2-}$ (Scheme 1).

Using equivalent amounts of tetrathiafulvalene (TTF) derivatives and $Co^{II}Cp_2$, we have isolated $[Cr^{III}(X_4SQ)_2(X_4Cat)]^-$ as the CT compounds.[5] The anions include two types of ligands, SQ and Cat, and show intramolecular intervalence transition (SQ ← Cat) near 4000 cm^{-1} in the solid state. One of the other redox isomers with mixed-charge ligands is a two-electron-reduced complex, $[Cr^{III}(X_4SQ)(X_4Cat)_2]^{2-}$, whose structure and properties in the solid state have been still unknown. The crystal and electronic structural comparison of these two isomers is of great interest regarding their assembled structures. It has been demonstrated that the TTF derivatives could not reduce $[Cr^{III}(X_4SQ)_2(X_4Cat)]^-$ to $[Cr^{III}(X_4SQ)(X_4Cat)_2]^{2-}$ because of the restricted reduction power ($E_{1/2}$ = 0.445 (TMTSF, tetramethyltetraselenafulvalene) and 0.520 (TMT-TTF, tetrakis(methylsulfanyl)tetrathiafulvalene) V (vs SCE)). On the other hand, $Co^{II}Cp_2$, widely used as a one-electron reductant, has stronger reduction power ($E_{1/2}$ = − 0.86 V).[6] On the basis of these chemical properties, we have first succeeded in the isolation of $[Cr^{III}(X_4SQ)(X_4Cat)_2]^{2-}$ as CT compounds with $[Co^{III}Cp_2]^+$. In addition, a 1:2 ($[Fe^{III}Cp_2]^+$:[Cr complex]) compound containing two redox isomers, $[Cr^{III}(Cl_4SQ)_2(Cl_4Cat)]^-$ and neutral $[Cr^{III}(Cl_4SQ)_3]^0$ complex, has been prepared using $Fe^{II}Cp_2$. The compound exhibits, in a sense, *intermolecular* mixed-valence state, indicative of a new class of molecular solid.

Experimental Section

Materials. All the chemicals were reagent grade. $Co^{II}Cp_2$ was obtained from Aldrich. Syntheses of **1** and **2** were carried out under a dry nitrogen atmosphere by use of standard Schlenk techniques with freshly distilled solvents. $Fe^{II}Cp_2$,[7] $Cr^{III}(X_4SQ)_3 \cdot 4C_6H_6$ (X = Cl and Br), and $(Co^{III}Cp_2)[Cr^{III}(Cl_4SQ)_2(Cl_4Cat)] \cdot C_6H_6$ (**3**) were prepared by the procedure described previously.[5]

Preparation of the Compounds. $(Co^{III}Cp_2)_2[Cr^{III}(Cl_4SQ)(Cl_4Cat)_2]$ (1). A 200 mL CH_2Cl_2 suspension containing $Cr^{III}(Cl_4SQ)_3 \cdot 4C_6H_6$ (1212 mg, 1.10 mmol) and $Co^{II}Cp_2$ (458 mg, 2.42 mmol) was refluxed for a day under dry nitrogen. The mixture was filtered and washed with CH_2Cl_2 several times, and the blue-violet product, which is a mono-anion, was completely extracted by Soxhlet extractor with 200 mL of CH_2Cl_2 for a day. The reddish-violet powder was isolated in 65% yield (830 mg). The product contains 1 mol of CH_2Cl_2 molecules. Found: C, 37.02; H, 1.88. $C_{39}H_{22}O_6Cl_{13}Co_2Cr$ requires C, 37.39; H, 1.77. The single crystal was obtained by careful diffusion of *n*-hexane to the filtrate obtained above. IR (KBr): 3370m, 3108m, 3078m, 2910w, 2832w, 2706w, 2515w, 2428w, 2182w, 1829w, 1718w, 1639w, 1445s, 1415s, 1373m, 1319m, 1289w, 1250s, 1124s, 1106s, 1057s, 1009m, 973s, 858s, 847m, 806m, 790s, 740m, 689m, 555m, 501w, 457s, 440w, and 420w cm^{-1}.

$(Co^{III}Cp_2)_2[Cr^{III}(Br_4SQ)(Br_4Cat)_2]$ (2). A 150 mL CH_2Cl_2 suspension containing $Cr^{III}(Br_4SQ)_3 \cdot 4C_6H_6$ (1584 mg, 0.969 mmol) and $Co^{II}Cp_2$ (385 mg, 2.036 mmol) was refluxed for a day under dry nitrogen. The mixture was filtered, washed with CH_2Cl_2 several times until the washings were no longer colored, and dried in a vacuum. The reddish-violet microcrystals were isolated in a 88% yield (1490 mg). A single crystal was obtained by careful diffusion of Et_2O to the filtrate obtained above. Found: C, 26.41; H, 1.25. $C_{38}H_{20}O_6Br_{12}Co_2Cr$ requires C, 26.83; H, 1.18. IR (KBr): 3371w, 3103m, 3089m, 2911w, 2846w, 2671w, 2509w, 2089w, 1810w, 1730w, 1632w, 1440s, 1415s, 1347w, 1297m, 1258s, 1234m, 1206w, 1134s, 1053s, 1008m, 929s, 857m, 846w, 820w, 752m, 740m, 708m, 624w, 600w, 544m, 500w, 459m, 423w, and 408w cm^{-1}.

$(Fe^{III}Cp_2)[Cr^{III}(Cl_4SQ)_2(Cl_4Cat)] \cdot C_6H_6$ (4). Single crystals of the compound were grown from a layered 50 mL of a carbon disulfide solution containing $Cr^{III}(Cl_4SQ)_3 \cdot 4C_6H_6$ (101 mg, 0.0916 mmol) and 50 mL of C_6H_6 solution containing $Fe^{II}Cp_2$ (17 mg, 0.0916 mmol). Blue violet cubic crystals were obtained after 1 week. Found: C, 38.71; H, 1.64. $C_{34}H_{16}O_6Cl_{12}CrFe$ requires C, 38.75; H, 1.53. IR (KBr): 3102w, 2726w, 2534w, 1476m (C_6H_6), 1435m, 1416m, 1307m, 1248w, 1179s, 1103s, 1049s, 1011m, 980s, 847m, 797s, 785s, 691m, 677s (C_6H_6), 624w, 608w, 582w, 545w, 522w, 443s, and 417s cm^{-1}.

$(Fe^{III}Cp_2)[Cr^{III}(Br_4SQ)_2(Br_4Cat)] \cdot CS_2$ (5). Single crystals of the compound were grown from a layered 300 mL of a carbon disulfide solution containing $Cr^{III}(Br_4SQ)_3 \cdot 4C_6H_6$ (500 mg, 0.306 mmol) and 200 mL of *n*-hexane solution containing $Fe^{II}Cp_2$ (57 mg, 0.306 mmol). Blue violet cubic crystals were obtained after 1 week. Found: C, 22.09; H, 0.76. $C_{29}H_{10}O_6Br_{12}CrFeS_2$ requires C, 21.97; H, 0.64. IR (KBr): 3100w, 2458w, 1450m, 1430m, 1418m, 1349w, 1310w, 1288w, 1245m, 1232m, 1210w, 1166s, 1120s, 1106s, 1051m, 1009w, 933s, 850m, 752m, 699m, 623w, 559w, 503w, and 405 cm^{-1}.

$(Fe^{III}Cp_2)[Cr^{III}(Cl_4SQ)_2(Cl_4Cat)][Cr^{III}(Cl_4SQ)_3]_2$ (6). Single crystals of the compound were grown from a layered 80 mL of a carbon disulfide solution containing $Cr^{III}(Cl_4SQ)_3 \cdot 4C_6H_6$ (331 mg, 0.30 mmol) and 80 mL of *n*-hexane solution containing $Fe^{II}Cp_2$ (28 mg, 0.15 mmol). Violet crystals were obtained after 1 week. Found: C, 31.20; H, 0.74. $C_{46}H_{10}O_{12}Cl_{12}Cr_2Fe$ requires C, 31.30; H, 0.57. IR (KBr): 3109w, 2722w, 2517w, 1472m, 1456s, 1446s, 1416w, 1382w, 1337m, 1310m, 1276m, 1248w, 1216s, 1117s, 1104s, 1051sh, 1013w, 990s, 979s, 856w, 824m, 799s, 786m, 693m, 581w, 529w, 447s, 433s, and 416m cm^{-1}.

Physical Measurements. Infrared spectra for KBr pellets were recorded on a Perkin-Elmer system 2000 FT-IR spectrometer and absorption spectra on a Hitachi U-3500 spectrophotometer over the range 3130−33000 cm^{-1} at 296 K. Magnetic susceptibilities were recorded over the temperature range 1.9−350 K at 1 T with a superconducting quantum interference device (SQUID) susceptometer (Quantum Design, San Diego, CA) interfaced with a HP Vectra computer system. All the values were corrected for diamagnetism that were calculated from Pascal's table.[8]

Crystallographic Data Collection and Refinement of Structures. For compound **1**, data collection was made on a Rigaku AFC7R diffractometer with graphite-monochrometed Mo Kα radiation and a rotating anode generator at 296 K. The crystal was mounted in a thin-walled glass capillary with mother liquor. Unit cell constants and an orientation matrix for data collection were obtained from least-squares refinements using the setting angles of 25 carefully centered reflections in the range $6.79° < 2\theta < 14.45°$. Independent reflections of 6121 were obtained, and 1815 of them with $I > 2\sigma(I)$ were considered "observed" and used in the full-matrix least-squares refinements. For compounds **2** and **4**−**6**, the measurements were performed with Mo Kα radiation employing a graphite monochromator at 296 K on a Rigaku mercury diffractometer with CCD two-dimensional detector. The sizes of the unit cells were calculated from the reflections collected

(4) (a) Mayerle, J. J.; Torrance, J. B. *Acta Crystallogr., Sect. B* **1981**, *B37*, 2030. (b) Nakasuji, K.; Sasaki, M.; Kotani, T.; Murata, I.; Enoki, T.; Imaeda, K.; Inokuchi, H.; Kawamoto, A.; Tanaka, J. *J. Am. Chem. Soc.* **1987**, *109*, 6970.
(5) Chang, H.-C.; Ishii, T.; Kondo, M.; Kitagawa, S. *J. Chem. Soc., Dalton Trans.* **1999**, 2467.
(6) Koelle, U.; Khouzami, F. *Angew. Chem., Int. Ed. Engl.* **1980**, *19*, 640.
(7) King, R. B.; Bisnette, M. B. *J. Organomet. Chem.* **1967**, *8*, 287.
(8) Kahn, O. *Molecular Magnetism*; VCH: New York, 1993.

Table 1. Crystallographic and Refinement Data for **1**, **2**, and **4**−**6**

	1	**2**	**4**	**5**	**6**
formula	$C_{38}H_{20}O_6Cl_{12}Co_2Cr$	$C_{38}H_{20}O_6Br_{12}Co_2Cr$	$C_{34}H_{16}O_6Cl_{12}CrFe$	$C_{29}H_{16}O_6Br_{12}CrFeS_2$	$C_{46}H_{10}O_{12}Cl_{24}Cr_2Fe$
fw	1167.87	1701.28	1053.78	1585.21	1765.29
cryst syst	monoclinic	monoclinic	triclinic	triclinic	monoclinic
space group	$P2_1/n$ (No. 14)	$P2_1/n$ (No. 14)	$P\bar{1}$ (No. 2)	$P\bar{1}$ (No. 2)	$C2_1/c$ (No. 15)
a, Å	9.760(5)	13.472(1)	10.9364(3)	11.075(1)	23.904(2)
b, Å	31.535(6)	20.5443(5)	13.939(2)	11.2691(7)	17.807(3)
c, Å	14.191(7)	17.6961(3)	14.3387(8)	16.899(2)	16.6538(4)
α, deg			82.036(3)	86.120(3)	
β, deg	108.08(4)	110.4321(4)	75.470(2)	80.609(1)	123.2850(5)
γ, deg			67.498(1)	73.578(1)	
Z	4	4	2	2	4
V, Å3	4152(3)	4589.8(5)	1952.2(3)	1995.3(3)	5925(1)
ρ_{calcd}, g/cm^3	1.868	2.462	1.793	2.638	1.979
μ, cm^{-1}	18.66	114.70	15.15	128.33	17.43
T, K	296	296	296	296	296
λ(Mo Kα), Å	0.71069	0.71069	0.71069	0.71069	0.71069
R_{int}	0.042	0.025	0.012	0.022	0.020
R, R_w	0.102, 0.113	0.038, 0.041	0.034, 0.052	0.049, 0.054	0.042, 0.045

[a] $R = \sum||F_o| - |F_o||/\sum|F_o|$, $R_w = [\sum(|F_o| - |F_o|)^2/\sum w|F_o|^2)]^{1/2}$.

Scheme 2

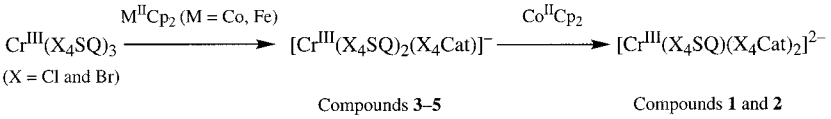

on the setting angles of four frames by changing ω by 0.5° for each frame. Two different χ settings were used and ω was changed by 0.5° per frame. Intensity data were collected in 480 frames with an ω scan width of 0.5° and exposure times 150, 25, 60, and 120 s for **2** and **4**−**6**, respectively. Empirical absorption correction using the program REQABA[9] was performed for all the data. All the crystal data are summarized in Table 1. The structures were solved by direct methods[10] and expanded using Fourier techniques.[11] The final cycles of the full-matrix least-squares refinements were based on the observed reflections ($I > 3\sigma(I)$). All the calculations were performed using the teXsan crystallographic software package of Molecular Structure Corporation.[12] For compound **1**, all the atoms except for Co(1), Co(2), and Cr(1) were refined isotropically. For compounds **2** and **4**−**6** the non-hydrogen atoms were refined anisotropically and all the hydrogen atoms were placed in the idealized positions, but their parameters were not refined. In compound **2** the disorder of the Cp ring containing C(34)−C(38) was found at the final stage, and thus its atom positions were isotropically refined under a rigid condition.

Results and Discussion

Syntheses. Complexes $Cr^{III}(X_4SQ)_3$ undergo electrochemical reduction, capable of receiving three electrons on the ligand moieties, and affording $[Cr^{III}(X_4SQ)_2(X_4Cat)]^-$, $[Cr^{III}(X_4SQ)(X_4Cat)_2]^{2-}$, and $[Cr^{III}(X_4Cat)_3]^{3-}$.[13] On the other hand, $M^{II}Cp_2$ (M = Co and Fe) are oxidized to diamagnetic $[Co^{III}Cp_2]^+$ and paramagnetic $[Fe^{III}Cp_2]^+$ cations, respectively. In general, the CT reaction strongly depends on the redox potentials of the donor and the acceptor molecules used. It is worth noting that the oxidation potential of $Co^{II}Cp_2$ (−0.86 V vs SCE) is extremely low in comparison with those of $Fe^{II}Cp_2$ (0.49 V) and TTF derivatives (0.445 (TMTSF), 0.520 (TMT-TTF) V), exhibiting strong reducing power. The stoichiometric mixing of metallocene causes a CT reaction to give 1:1 (**3**−**5**) compounds (Scheme 2). The second reduction of the ligand also occurs in the presence of 2 mol of the $Co^{II}Cp_2$ to form 2:1 compounds (**1** and **2**).

Interestingly, solvents used influence crystal structures where the stoichiometric ratios of the cation to anion are 1:1 to 1:2; a combination of C_6H_6/CS_2 affords 1:1:C_6H_6 compound **4**, while *n*-C_6H_{12}/CS_2 gives 1:2 ([$FeCp_2$]:[Cr complex]) compound **6**. This is associated with a stacking nature of the C_6H_6 molecule, which plays an important role in stabilizing the overall packing structures where a mixed-stack form preferentially occurs (see Supporting Information and ref 5).

Molecular Crystal Structures. Figures 1−4 show ORTEP[14] drawings of **1** and **4**−**6** with the atom-numbering schemes. At 296 K, compound **4** is isostructural with previously reported $(Co^{III}Cp_2)[Cr^{III}(Cl_4SQ)_2(Cl_4Cat)]\cdot C_6H_6$ (**3**).[5] In compounds **1** and **2**, there are two crystallographically independent $CoCp_2$ molecules, while compounds **4**−**6** contain one crystallographically independent $FeCp_2$ molecule. The iron atom of **6** is located at the special position ($^3/_4$, $-^1/_4$, $^1/_2$), only one of the Cp ring moieties being unique. All the compounds contain one homoleptic chromium complex, $[Cr(C_6O_2X_4)_3]$ (X = Cl for **1**, **4**, and **6** and Br for **2** and **5**), where the three coordinated ligands are labeled as **I**, **II**, and **III**. Compounds **4** and **5** are solvated with C_6H_6 and CS_2, respectively.

$[M^{III}Cp_2]^+$. The average bond distances and angles relevant to each MCp_2 molecule in **1**−**6** are listed in Table 2 together with those of $[M^{II}Cp_2]^0$ and $[M^{III}Cp_2]^+$ (M = Co and Fe) reported so far. The Co−C bond distances of **1** and **2** range from 1.96(4) to 2.09(3) Å, averaged to 2.01(4) (**1**) and 2.01(1) (**2**) Å, respectively. The C−C bond distances range from 1.30(5)

(9) Jacobson, R. A. *REQABA Empirical Absorption Correction Version 1.1-03101998*: Molecular Structure Corp.: The Woodlands, TX, 1996−1998.
(10) Altomare, A.; Burla, M. C.; Camalli, M.; Cascarano, M.; Giacovazzo, C.; Guagliardi, A.; Pilidori, G. *J. Appl. Crystallogr.* **1994**, *27*, 435.
(11) Beurskens, P. T.; Admiraal, G.; Beurskens, G.; Bosman, W. P.; de Gelder, R.; Israel, R.; Smits, J. M. M. The DIRDIF-94 program system. Technical Report of the Crystallography Laboratory; University of Nijmegen: Nijmegen, The Netherlands, 1994.
(12) *teXsan: Crystal Structure Analysis Package*; Molecular Structure Corporation: The Woodlands, TX, 1985, 1992.
(13) Downs, H. H.; Buchanan, R. M.; Pierpont, C. G. *Inorg. Chem.* **1979**, *18*, 1736.
(14) Johnson, C. K. *ORTEP II*; Report ORNL-5138; Oak Ridge National Laboratory: Oak Ridge, TN, 1976.

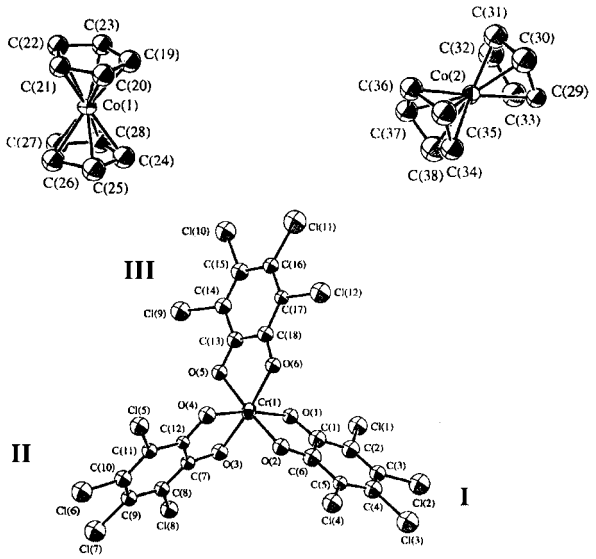

Figure 1. An ORTEP drawing of **1** with hydrogen atoms omitted (showing 30% isotropic thermal ellipsoids). Crystallographically independent ligands are designated **I**, **II**, and **III**. The atomic numbering scheme for **2** is the same as that for **1**.

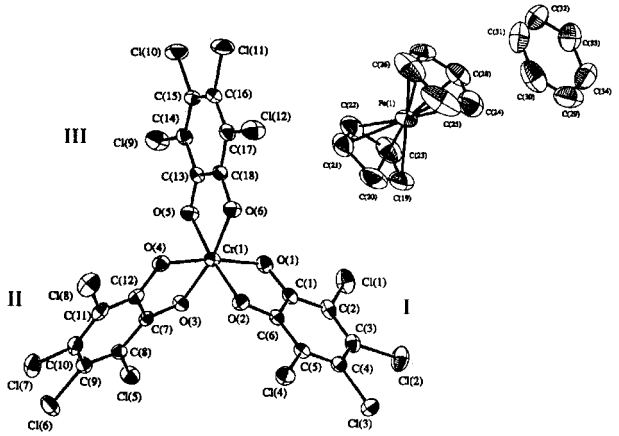

Figure 2. An ORTEP drawing of **4** with hydrogen atoms omitted (showing 30% anisotropic thermal ellipsoids). Crystallographically independent ligands are designated **I**, **II**, and **III**.

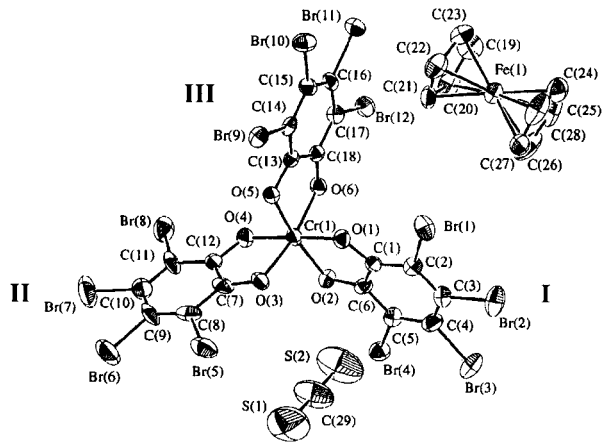

Figure 3. An ORTEP drawing of **5** with hydrogen atoms omitted (showing 30% anisotropic thermal ellipsoids). Crystallographically independent ligands are designated **I**, **II**, and **III**.

to 1.52(5) Å averaged to be 1.39(5) (**1**) and 1.39(2) (**2**) Å, respectively. These distances are shorter than those of $[Co^{II}Cp_2]^0$ (2.096(8) and 1.41(1) Å)[15a] and in accord with those of

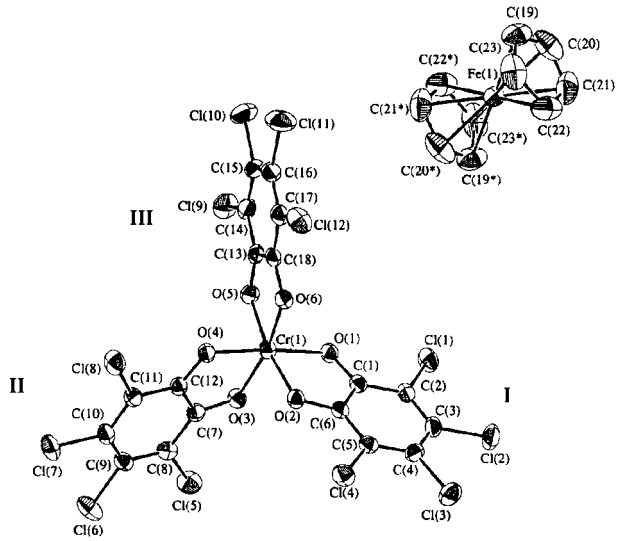

Figure 4. An ORTEP drawing of **6** with hydrogen atoms omitted (showing 30% anisotropic thermal ellipsoids). The $FeCp_2$ molecule has centroids coincident with crystallographic symmetry. Three crystallographically independent ligands are designated **I**, **II**, and **III**.

Table 2. Comparison of Average Intramolecular Bond Distances (Å) for $[M^{III}Cp_2]^+$ Found in **1**−**6** with $[M^{II}Cp_2]^0$ (M = Co, Fe) and $[M^{III}Cp_2]^+$

compound	M−C	C−C
1	2.00(4), 2.03(4)	1.38(4), 1.40(5)
2	2.01(1), 2.01(1)	1.38(3), 1.39(3)
3[a]	2.005(9)	1.375(2)
$[Co^{II}Cp_2]^0$ [b]	2.096(8)	1.41(1)
$[Co^{III}Cp_2]^+$ [c]	2.023(5)	1.402(6)
4	2.066(6)	1.38(1)
5	2.06(2)	1.37(3)
6	2.056(7)	1.36(1)
$[Fe^{II}Cp_2]^0$ [d]	2.033	1.389
$[Fe^{III}Cp_2]^+$ [e]	2.08(1)	1.40(2)

[a] Reference 5. [b] Reference 15a. [c] Reference 15b. [d] Reference 15c. [e] Reference 15d.

previously reported distances of 2.023(5) and 1.402(6) Å for $[Co^{III}Cp_2]^+$,[15b] respectively. A similar trend has been found in those of **3**.[5]

The Fe−C bond distances fall within the ranges 2.023(6)−2.094(5), 2.03(2)−2.12(2), and 2.038(7)−2.073(6) Å for **4**, **5**, and **6**, respectively, and the average values are slightly longer than 2.033 Å found for $[Fe^{II}Cp_2]^0$,[15c] showing a similar trend for $[Fe^{III}Cp_2]^+$ reported so far.[15d] The crystal structures of the cationic moieties clearly indicate that the $[M^{II}Cp_2]^0$ molecules are oxidized to $[M^{III}Cp_2]^+$ in all the compounds.

Chromium Complexes. The geometry of the chromium ion is all the distorted octahedrons with six oxygen atoms from the three bidentate ligands **I**−**III**. In Table 3 the Cr−O, C−C, and C−O bond distances and O−Cr−O angles are listed in comparison with those of complexes $Cr^{III}(Cl_4SQ)_3\cdot CS_2\cdot 0.5C_6H_6$[3c] and **3**. The averaged Cr−O and C−C bond distances for the three ligand moieties of all the compounds, hereafter called total average, show constant values of 1.94 and 1.40 Å, respectively. For each compound, the differences in bond distances among the three ligands are in the ranges 0.01−0.032

(15) (a) Kemmitt, R. D. W.; Russell, D. R. *Comprehensive Organometallic Chemistry*; Pergamon: Oxford, 1982. (b) Sens, V. I.; Ruhlandt-Senge, K.; Müller, U. *Acta Crystallogr., Sect. C* **1992**, *C48*, 742. (c) Seiler, P.; Dunitz, J. D. *Acta Crystallogr., Sect. B* **1979**, *B35*, 1068. (d) Mammano, N. J.; Zalkin, A.; Landers, A.; Rheingold, A. L. *Inorg. Chem.* **1977**, *16*, 297.

Table 3. Intraligand and Total Average Bond Distances (Å) and Angles (deg) and Charge for Anionic $[Cr^{III}(X_4SQ)_{3-n}(X_4Cat)_n]^{n-}$ Complexes of **1**−**6** and $Cr^{III}(Cl_4SQ)_3 \cdot CS_2 \cdot {}^1/_2C_6H_6$

	ligand	**1**	**2**	**3**[b]	**4**	**5**	**6**	$Cr(Cl_4SQ)_3$[a]
Cr−O (Å)	**I**	1.95(2)	1.951(6)	1.933(3)	1.928(2)	1.922(9)	1.938(3)	
	II	1.96(2)	1.940(6)	1.936(3)	1.937(2)	1.954(10)	1.945(3)	
	III	1.96(2)	1.939(6)	1.955(3)	1.957(2)	1.945(8)	1.949(3)	
total av		1.96(2)	1.943(6)	1.941(3)	1.941(2)	1.940(10)	1.944(3)	1.949(5)
C−O (Å)	**I**	1.31(3)	1.33(1)	1.311(5)	1.313(4)	1.31(2)	1.305(5)	
	II	1.31(3)	1.32(1)	1.299(6)	1.300(4)	1.29(2)	1.286(5)	
	III	1.29(3)	1.310(10)	1.292(2)	1.291(4)	1.30(1)	1.286(6)	
total av		1.30(3)	1.32(1)	1.301(5)	1.301(4)	1.30(2)	1.292(6)	1.280(1)
C−C (Å)	**I**	1.39(4)	1.39(1)	1.392(7)	1.394(5)	1.40(2)	1.403(7)	
	II	1.39(4)	1.40(1)	1.397(7)	1.399(5)	1.41(2)	1.405(7)	
	III	1.40 (4)	1.40(1)	1.399(7)	1.402(5)	1.40(2)	1.405(7)	
total av		1.39(4)	1.40(2)	1.396(7)	1.398(5)	1.40(2)	1.404(7)	1.40(1)
O−Cr−O (deg)	**I**	83.2(9)	82.9(3)	83.3(1)	83.08(9)	83.2(4)	83.0(1)	
	II	83.1(9)	82.6(2)	82.7(1)	82.57(9)	81.2(4)	82.3(1)	
	III	82.4(8)	83.6(2)	81.9(1)	81.66(9)	82.4(4)	81.9(1)	
total av		82.9(9)	83.0(2)	82.6(1)	82.44(9)	82.3(4)	82.3(1)	81.8(2)
charge		−2	−2	−1	−1	−1	−1, 0[c]	0

[a] Reference 3e. [b] Reference 5. [c] Estimated from absorption spectra and magnetic susceptibility.

and 0.02−0.1 Å for Cr−O and C−C bond distances, respectively. In contrast, the total average C−O bond distances of **3**−**6** are in the range 1.292(6)−1.301(5) Å, which is elongated by approximately 0.2 Å from those of $Cr^{III}(Cl_4SQ)_3 \cdot CS_2 \cdot 0.5C_6H_6$. In particular, ligands **I** of **3**−**6** seem to have long C−O and short Cr−O bond distances when compared with other ligands **II** and **III**. On the other hand, compound **2** has the total average C−O bond distance 1.32(1) Å, which is longer by 0.02 Å than those of **3**−**6**. Similar trends are observed for the O−Cr−O angles, which are enlarged by the reduction of the SQ to the Cat,[16] that is, 81.8(2)° and 83.6(1)° for $Cr^{III}(Cl_4SQ)_3$ and $[Cr^{III}(Cat)_3]^{3-}$, respectively. In the present compounds, the total average O−Cr−O angles are larger by about 1.2° (**1** and **2**) and 0.6° (**4**−**6**) than that of $Cr^{III}(Cl_4SQ)_3$, respectively, indicating the reduction of the ligand moieties.

The oxidation numbers of the anionic complexes are responsible for the combination of SQ and Cat because of the inertness of the chromium center in the redox process.[13,16,17] On the basis of the ratio, $n[M^{III}Cp_2]^+/[Cr\ complex]$ (n = numbers of $[M^{III}Cp_2]^+$), the negative charge of the chromium anions can be assigned to −2 and −1 for **1**−**2** and **3**−**6**, respectively. In the former, the two SQ ligands are reduced to the corresponding Cat form to provide $[Cr^{III}(X_4SQ)(X_4Cat)_2]^{2-}$ while the $[Cr^{III}(X_4SQ)_2(X_4Cat)]^-$ in **3**−**5** results from the reduction of one SQ to the Cat.

There have been many *heteroleptic o*-dioxolene transition metal complexes which are X-ray crystallographically well-characterized: the charged states on the ligand are well-distinguished in a series of the complexes $[M^{III}(SQ)(Cat)(N\text{-}N)]$ (M = Fe and Co, N-N = bidentate nitrogen coligand)[18] and Cu^{II}(tetramethylethyldiamine)(9,10-phenBQ)(9,10-phenCat) (9,10-phenBQ = 9,10-phenanthrenebenzoquinone).[3d] In the case of *homoleptic* complexes, a similar distinction has been found only for Ni^{II}(3,6-DTBBQ)(3,6-DTBSQ)$_2$[19a] and Mn^{IV}(3,6-DTBSQ)$_2$(3,6-DTBCat) (DTB = di-*tert*-butyl).[19(b)] On the other hand, the differences in structural parameters among the three ligand moieties for **1**−**5** are still small in comparison with the

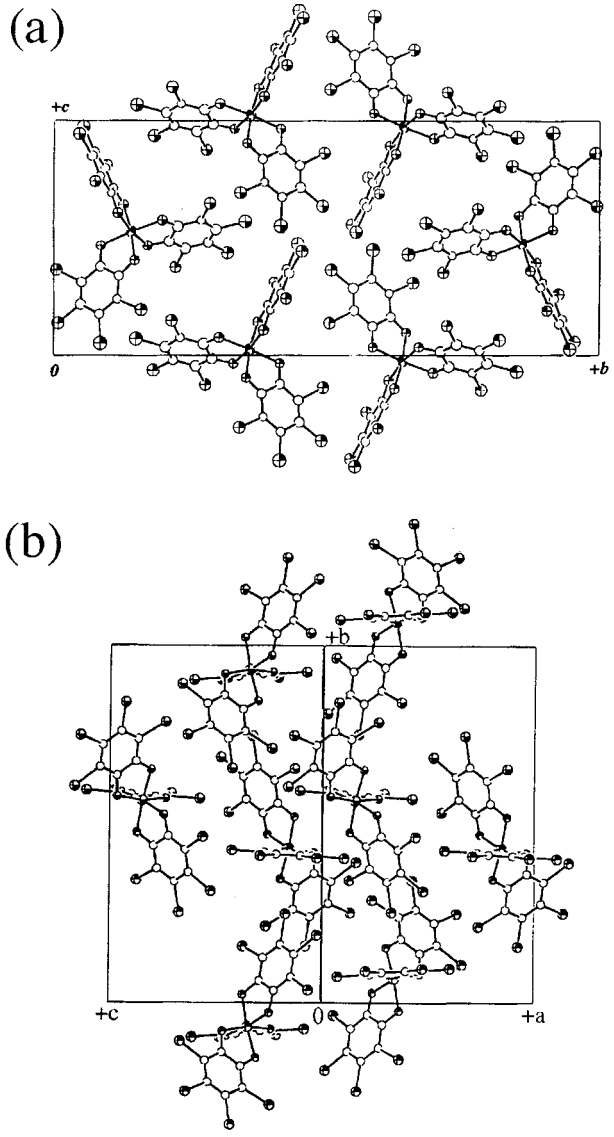

Figure 5. The crystal packing structures of $[Cr^{III}(X_4SQ)(X_4Cat)_2]^{2-}$ anions of (a) **1** and (b) **2**.

(16) Sofen, S. R.; Ware, D. C.; Cooper, S. R.; Raymond, K. N. *Inorg. Chem.* **1979**, *18*, 234.
(17) Buchanan, R. M.; Claflin, J.; Pierpont, C. G. *Inorg. Chem.* **1983**, *22*, 2552.
(18) (a) Buchanan, R. M.; Pierpont, C. G. *J. Am. Chem. Soc.* **1980**, *102*, 4951. (b) Attia, A. S.; Bhattacharya, S.; Pierpont, C. G. *Inorg. Chem.* **1995**, *34*, 4427. (c) Jung, O.-S.; Jo, D. H.; Lee, Y.-A.; J., C. B.; Pierpont, C. G. *Inorg. Chem.* **1997**, *36*, 19. (d) Jung, O.-S.; Pierpont, C. G. *Inorg. Chem.* **1994**, *33*, 2227.
(19) (a) Lange, C. W.; Pierpont, C. G. *Inorg. Chim. Acta* **1997**, *263*, 219. (b) Attia, A. S.; Pierpont, C. G. *Inorg. Chem.* **1998**, *37*, 3051.

Table 4. Parameters for Intermolecular Stacking Arrangements and X···X Contacts of the Anions of **1**, **2**, and **4**−**6**

compound	interplanar distance (Å)		intermolecular X···X contact distance (Å)			
1			Cl(2)···Cl(8*)[a]	3.47(1)	Cl(6)···Cl(10*)[b]	3.36(1)
2			Br(1)···Br(5*)[c]	3.819(2)	Br(6)···Br(10*)[d]	3.685(2)
			Br(2)···Br(7*)[c]	3.766(2)	Br(7)···Br(10*)[e]	3.897(2)
			Br(3)···Br(5*)[f]	3.873(2)	Br(8)···Br(11*)[g]	3.577(2)
			Br(6)···Br(8*)[h]	3.812(2)		
			intracolumn (Å)		intercolumn (Å)	
4	**I**···**I′**	3.521(4)	Cl(1)···Cl(9*)[i]	3.472(1)	Cl(3)···Cl(11*)[j]	3.454(1)
	II···**II′**	3.540(4)	Cl(2)···Cl(5*)[g]	3.588(2)	Cl(4)···Cl(10*)[k]	3.572(1)
			Cl(2)···Cl(7*)[l]	3.295(1)	Cl(7)···Cl(10*)[m]	3.245(1)
5	**II**···**II′**	3.63(2)	Br(4)···Br(7*)[c]	3.742(3)	Br(1)···Br(1*)[n]	3.513(3)
	III···**III′**	3.49(1)	Br(4)···Br(11*)[o]	3.699(2)	Br(2)···Br(10*)[n]	3.605(2)
			Br(8)···Br(10*)[d]	3.563(2)	Br(2)···Br(9*)[p]	3.619(2)
			Br(9)···Br(11*)[d]	3.861(2)	Br(3)···Br(5*)[p]	3.595(3)
					Br(3)···Br(11*)[o]	3.794(2)
6	**I**···**I′**	3.557(6)	Cl(2)···Cl(2*)[q]	3.467(3)	Cl(4)···Cl(4*)[r]	3.492(3)
	III···**III′**	3.583(7)	Cl(3)···Cl(12*)[s]	3.588(2)	Cl(5)···Cl(12*)[t]	3.529(2)
	I···**II′**	3.592(6)			Cl(6)···Cl(11*)[u]	3.189(2)
					Cl(10)···Cl(10*)[f]	3.549(7)

[a] (x, $^1/_2 - y$, $^1/_2 + z - 1$). [b] (x, y, $z + 1$). [c] ($-x + 1$, $-y$, $-z$). [d] ($-x + 1$, $-y$, $-z + 1$). [e] ($^1/_2 - x + 1$, $^1/_2 + y - 1$, $-z + 1$). [f] ($x + 2$, $y + 2$, $z + 2$). [g] ($-x + 2$, $-y$, $-z + 1$). [h] ($^1/_2 + x - 1$, $^1/_2 - y - 1$, z). [i] ($-x + 1$, $-y + 1$, $-z + 1$). [j] ($-x + 2$, $-y + 1$, $-z + 1$). [k] ($x + 1$, $y - 1$, z). [l] (x, y, $z - 1$). [m] ($-x + 1$, $-y + 1$, $-z + 2$). [n] ($-x$, $-y + 1$, $-z + 1$). [o] ($-x$, $-y$, $-z + 1$). [p] ($x - 1$, y, z). [q] ($-x + 1$, y, $^1/_2 - z + 1$). [r] ($-x + 1$, y, $^1/_2 - z$). [s] ($^1/_2 + x$, $^1/_2 - y - 1$, $^1/_2 + z$). [t] ($x + 6$, $y + 6$, $z + 6$). [u] ($x + 5$, $y + 5$, $z + 5$).

estimated standard deviations (Table 3). This is because a crystallographic disorder often takes place and prevents the distinction between the SQ and the Cat form from the structural parameters. Therefore the distinction of the charged state for the three ligands is restricted as far as X-ray crystallographic data are used. Fortunately, spectroscopic and magnetic susceptibility data show localized electronic structures of $[Cr^{III}(X_4SQ)(X_4Cat)_2]^{2-}$ and $[Cr^{III}(X_4SQ)_2(X_4Cat)]^{-}$ for **1**−**2** and **3**−**5**, respectively. Thus, hereafter, the anionic chromium complexes are written as $[Cr^{III}(X_4SQ)(X_4Cat)_2]^{2-}$ (**1**−**2**) and $[Cr^{III}(X_4SQ)_2(X_4Cat)]^{-}$ (**3**−**5**) without the assignment of the oxidation states to each ligand.

For compound **6**, the crystallographic data appears to impart the charge of −1 to the two molecules of chromium complexes. However, alternative assignment for the charge on the chromium complex could be established by absorption spectroscopy and temperature-dependent magnetic susceptibility. The details are shown below.

Crystal Packing Structures. Compounds 1 and 2. Figure 5 shows crystal packing diagrams of **1** and **2**. Each chromium complex anion is separated by $[Co^{III}Cp_2]^+$, where the planes of the Cp rings are not parallel to those of the ligands of the anion. The two (**1**) and seven (**2**) pairs of intermolecular X···X contacts between the halogen atoms of the adjacent anions are observed within the sum of van der Waals radii (3.60 and 3.90 Å for Cl···Cl and Br···Br, respectively) (Table 4). However, both structures do not show the stacking arrangements of the $[Co^{III}Cp_2]^+$ and/or $[Cr^{III}(X_4SQ)(X_4Cat)]^{2-}$. This is associated with the large electrostatic repulsion because of their −2 charged states. This aspect of the assemblage is quite different from those of the following compounds in which the anion makes intermolecular stacking arrangements.

Compounds 4−6. An interesting feature of **4**−**6** is the one-dimensional columnar structure of the $[Cr^{III}(X_4SQ)_2(X_4Cat)_2]^{-}$. Figure 6a−c shows three types of one-dimensional columnar structures of **4**−**6**, respectively. Each column is characterized by alternating arrangements of the Δ and Λ enantiomers, indicating stacking linkage between [**I**···**I′**] and [**II**···**II′**] for **4**. Similarly, [**II**···**II′**]/[**III**···**III′**] and [**I**···**I′**]/[**III**···**III′**] for **5** and **6** are found, respectively. In **4**, the planes of the remaining ligand (**III**) are perpendicular to the direction of the column (Figure 6a), while the corresponding ligands **I** and **II** for **5** and **6**, respectively, are inclined with respect to the perpendicular plane of the main axis of the column; these are the [001] (**5**) and [101] (**6**) directions. Figure 7a−f illustrates the intermolecular overlap modes of the ligand moieties where the view direction is normal to the least-squares plane of one ligand, and the mean interplanar distances are listed in Table 4. Among the six pairs, the five pairs of Figure 7a and Figure 7c−f have a well-overlapping region regarding each six-membered ring, irrespective of a slight slip. The mean interplanar distances are in the range 3.49(1)−3.63(2) Å (Table 4), which are slightly larger than 3.22 (Cl), 3.47 (Cl), and 3.37 (Br) Å found for CT compounds of *p*-X_4BQ.[4,20] For ligand **II** of **4** (Figure 7b), the adjacent ligands exhibit a poor overlap, however, the chlorine atoms sitting over the adjacent six-membered ring.

In the case of **6**, the neighboring columns are linked to each other through the stacking formation of the ligand **I** and ligand **II′**, forming a two-dimensional sheet structure of the anions in the *ac*-plane (Figure 6d). The sitting mode of ligands **I** and **II′** is shown in Figure 7g, where C(2) and C(10*) atoms of six-membered rings of each ligand are overlapped with interplanar distance 3.592(6) Å. All the stacking arrangements found in **1**−**6** occur between the crystallographically equivalent ligands except for the pair of ligands **I** and **II′** of **6**. In addition to the ligand stacking arrangements, X···X contacts between neighboring anions are found through and between the columns (Table 4).

Physical Properties. Infrared Spectra and Electric Conductivity. The spectral region between 1500 and 1000 cm^{-1} contains strong bands associated with the C−O and C−C stretching modes that are sensitive to the charge of the ligand moieties.[21] Figure 8 shows the spectra of **1**, **4**, and **6**, together with that of $Cr^{III}(Cl_4SQ)_3 \cdot 4C_6H_6$, which shows sharp bands at 1461 and 1447 cm^{-1}, characteristic for the SQ.[22] For compound **4**, two bands at 1435 and 1416 cm^{-1} are observed, indicating

(20) Konno, M.; Kobayashi, H.; Marumo, F.; Saito, Y. *Bull. Chem. Soc. Jpn.* **1973**, *46*, 1987.
(21) (a) Hartl, F.; Stufkens, D. J.; Vleck, J. A. *Inorg. Chem.* **1992**, *31*, 1687. (b) Hartl, F.; Vleck, J. A.; Stufkens, D. J. *Inorg. Chim. Acta* **1992**, *192*, 25.
(22) Pierpont, C. G.; Downs, H. H.; Rukavina, T. G. *J. Am. Chem. Soc.* **1974**, *96*, 5573.

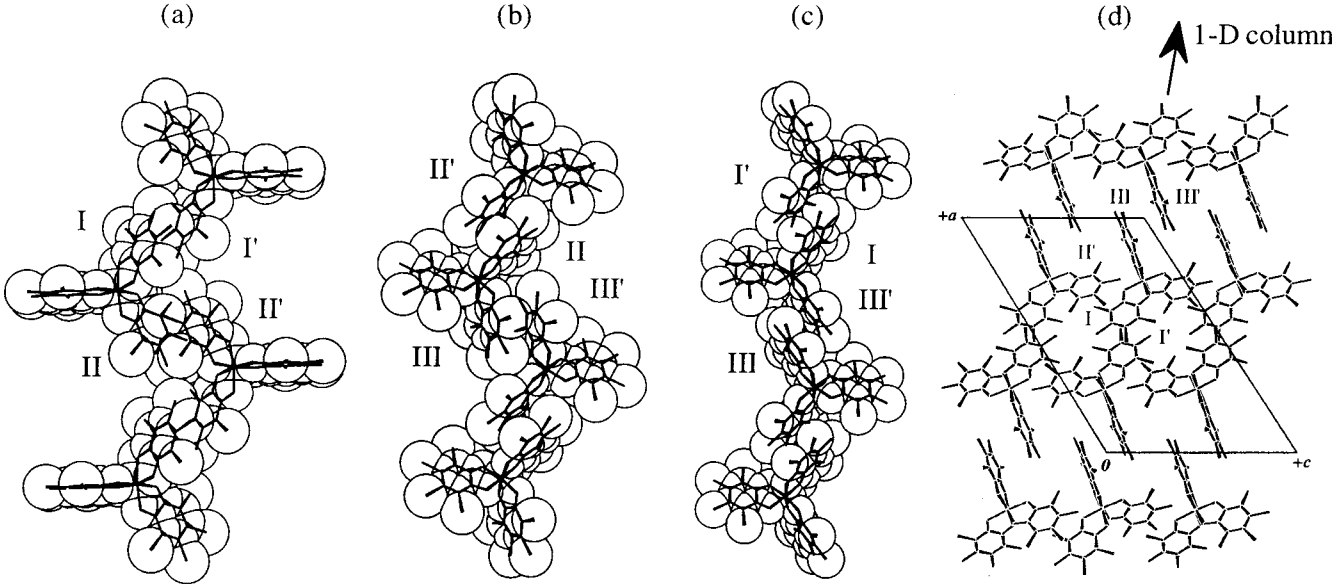

Figure 6. Space-filling representation of one-dimensional chain structures of $[Cr^{III}(X_4SQ)_2(X_4Cat)]^-$ anions found in (a) **4**, (b) **5**, and (c) **6**. (d) Two-dimensional anionic sheet of **6**.

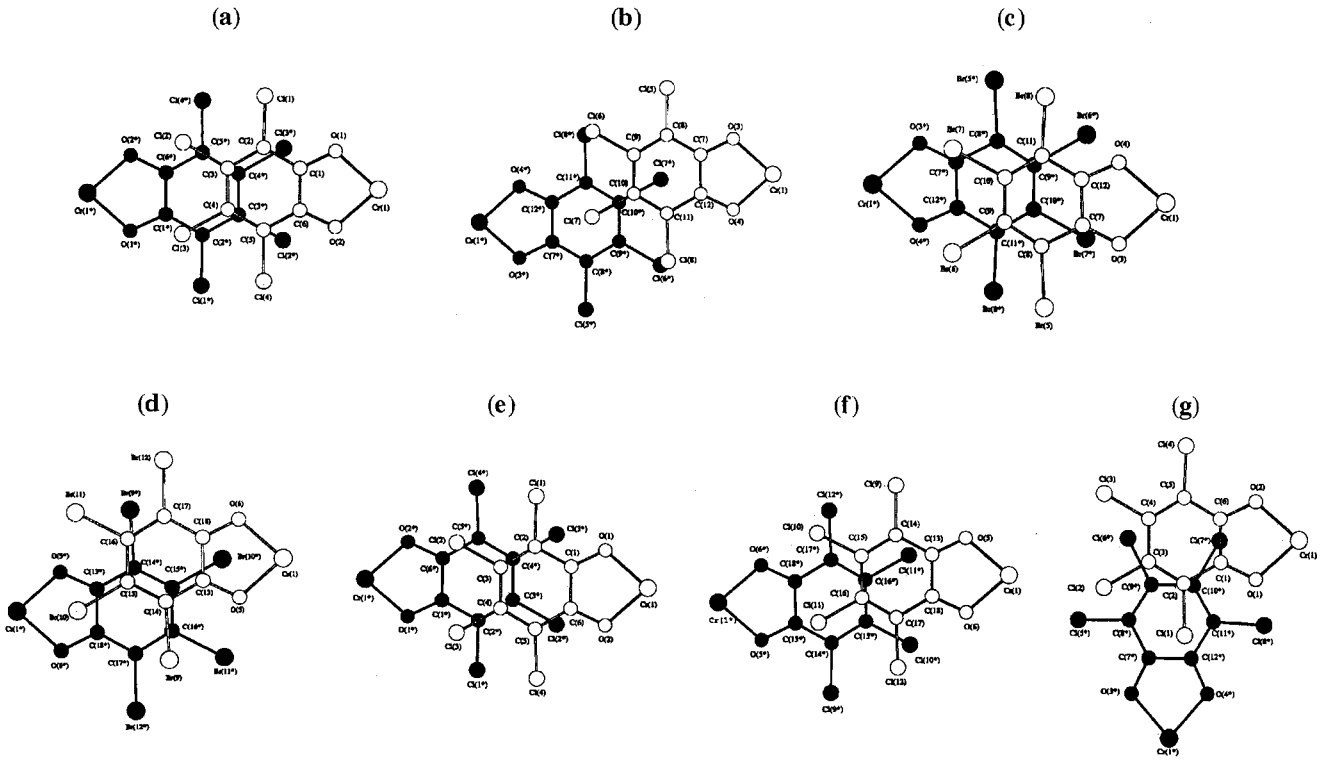

Figure 7. Intrachain ligand overlap modes of (a) **I···I′** (**4**), (b) **II···II′** (**4**), (c) **II···II′** (**5**), (d) **III···III′** (**5**), (e) **I···I′** (**6**), and (f) **III···III′** (**6**), and (g) interchain interaction **I···II′** (**6**). The stacking view projected down to a vector normal to the least-squares plane of the ligands drawn with white circles.

the presence of the SQ (Figure 8c). In addition, a new strong broad band appears at 1100 cm^{-1}, which is assigned to the C−O vibration mode of Cat.[23] This is consistent with the structure of $[Cr^{III}(Cl_4SQ)_2(Cl_4Cat)]^-$. Similar bands are observed for **3** and **5**, indicating that both SQ and Cat forms are present in **3**−**5**, supporting $[Cr^{III}(X_4SQ)_2(X_4Cat)]^-$ representation. The spectral patterns of **1** and **2** are quite similar to those of **3**−**5** in which characteristic bands for the SQ and the Cat are observed (Figure 8b).

For compound **6**, as well as other compounds, the presence of the mixed-valence ligands could be confirmed from the bands at 1440 (SQ) and 1100 (Cat) cm^{-1} (Figure 8d). In addition, the spectrum for **6** is just a superposition of the spectra of $Cr^{III}(Cl_4SQ)_3\cdot 4C_6H_6$ (Figure 8a) and **4** (Figure 8c). The bands near 1445, 1340, 1275, 990, 820, and 435 cm^{-1} are commonly found in $Cr^{III}(Cl_4SQ)_3\cdot 4C_6H_6$ and **6**, while the bands near 1310, 1100, 1050, 980, 850, 785, 450, and 420 cm^{-1} are commonly observed in **4** and **6**. The former and latter sets indicate that the two species $[Cr^{III}(Cl_4SQ)_2(Cl_4Cat)]^-$ and $[Cr^{III}(Cl_4SQ)_3]^0$ exist in **6**, though the crystallographic analysis shows one chromium species. Therefor, an *intermolecular* mixed-valence state occurs

(23) (a) Lynch, M. W.; Valentine, M.; Hendrickson, D. N. *J. Am. Chem. Soc.* **1982**, *104*, 6982. (b) Cass, M. E.; Gordon, N. R.; Pierpont, C. G. *Inorg. Chem.* **1986**, *25*, 3962.

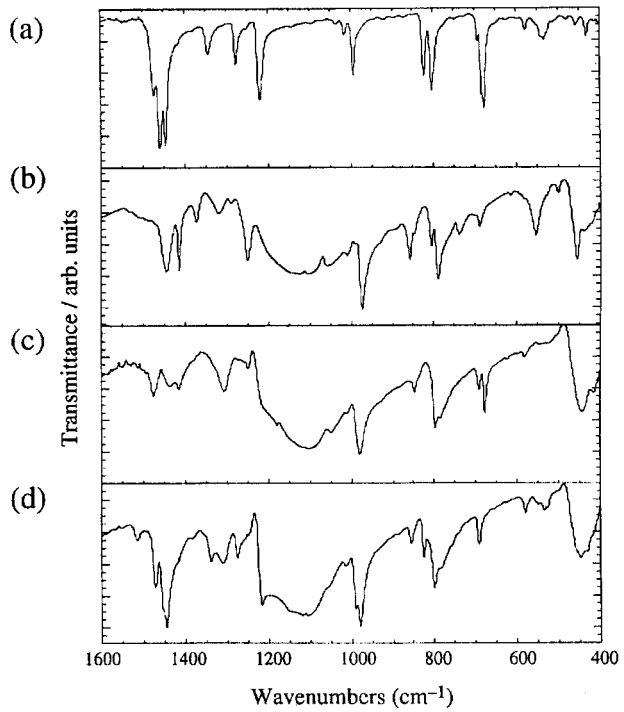

Figure 8. FT-IR spectra (KBr pellets) of (a) $Cr^{III}(Cl_4SQ)_3 \cdot 4C_6H_6$, (b) **1**, (c) **4**, and (d) **6**.

in **6** where the rate of intermolecular electron exchange is slower than the IR time scale.

Electrical conductivity is representative of physical properties for the mixed-valence molecular assemblies. Interestingly, a compacted pellet of **6** shows conductivity $\sigma_{295K} = 1.9 \times 10^{-3}$ S·cm^{-1}. The conductivity could be explained by the presence of the mixed-valence chromium complexes together with their interactions in the crystal phase. This is the first report regarding the isolation of an intermolecular mixed-valence molecular assembly derived from *o*-dioxolene complexes.

Electronic Absorption Spectra of Solution. Since all the CT compounds are soluble in CH_2Cl_2, we can use UV−vis−near-IR−IR absorption spectroscopy to confirm the oxidation states of the chromium complexes. Figure 9a,b shows absorption spectra of **1**, **4**, and **6** in the two regions 10000−30000 (region A) and 3000−10000 cm^{-1} (region B). In region A (Figure 9a), all the compounds commonly show the bands near 12500, 14700, and 21700 cm^{-1}, which are diagnostic of semiquinonate/catecholate chromium complexes.[16,17] The spectra can be classified into three groups from the spectral patterns, (type 1) **1** and **2**, (type 2) **3**−**5**, and (type 3) **6**; the spectra of type 1 are characterized by the band at 14700 (**1**) and 14500 (**2**) cm^{-1} with the intensities of ϵ = 2000 (**1**) and 3380 (**2**) M·cm^{-1}, respectively, which are weaker than those of types 2 and 3, ϵ = 4490−7130 M·cm^{-1}. In addition, absence of the shoulder near 11400 cm^{-1} found in types 2 and 3 is also recognized. The spectra of type 1 are identical to that reported by Sofen et al.[16] for electrochemically generated $[Cr^{III}$(3,5-DTBSQ)(3,5-DTBCat)$_2]^{2-}$ anion with respect to the number and position (ν_{max}) of observed transitions, indicating the formation of $[Cr^{III}(X_4SQ)(X_4Cat)_2]^{2-}$ (X = Cl (**1**) and Br (**2**)) anions, while the characteristics of type 2 are the bands near 15900 cm^{-1} with intensities 4460−8480 M^{-1}·cm^{-1} together with shoulders at 11400 cm^{-1}. These features correspond to that of $[Cr^{III}$(3,5-DTBSQ)$_2$(3,5-DTBCat)$]^-$ anion,[28] indicating the existence of

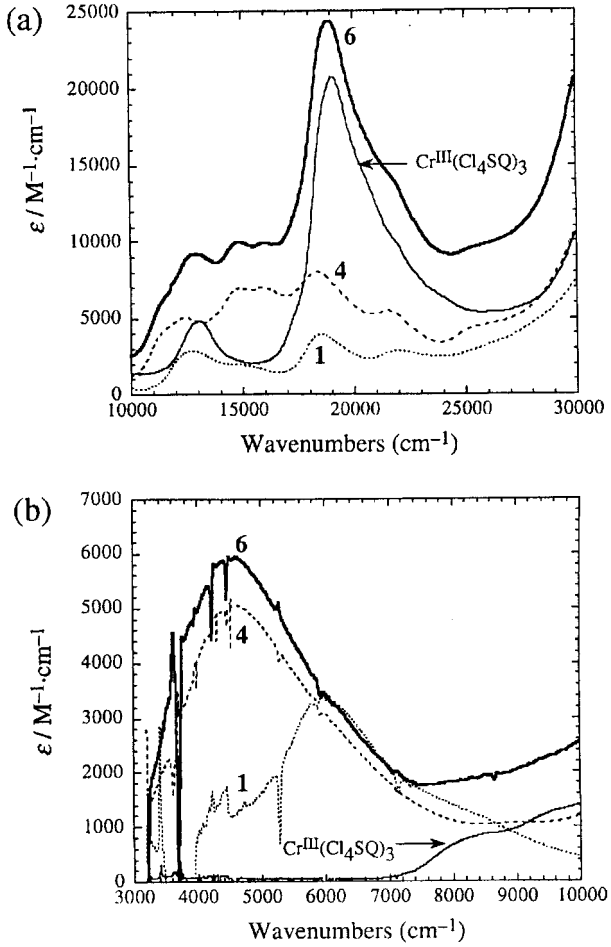

Figure 9. Electronic absorption spectra of **1** (···), **4** (---), **6** (—), and $Cr^{III}(Cl_4SQ)_3 \cdot 4C_6H_6$ (−) in CH_2Cl_2 at 296 K. The spectrum of **2** is similar to that of **1**, while those of **3** and **5** are similar to that of **4** (see Supporting Information).

$[Cr^{III}(X_4SQ)_2(X_4Cat)]^-$ for **3**−**5**. As well as **3**−**5**, compound **6** (type 3) shows common absorption bands at 11400, 14800, 16000, and 22000 cm^{-1}, and the characteristic bands at 12900 and 18900 cm^{-1} are found. It is noteworthy that these two band positions are very similar to 13000 and 19000 cm^{-1} found for $Cr^{III}(Cl_4SQ)_3 \cdot 4C_6H_6$. These results exhibit that compound **6** contains two types of chromium complexes, $[Cr^{III}(Cl_4SQ)_2(Cl_4Cat)]^-$ and $[Cr^{III}(Cl_4SQ)_3]^0$, and reflect the localized nature of the electronic structures of both forms in the solution.

As shown in Figure 9b, compounds **1**−**6** show characteristic broad intense absorption bands in the near-IR to IR region with several overtone vibrational transitions, whereas $[Cr^{III}(X_4SQ)_3]^0$ exhibits no absorption bands in the region 3000−7000 cm^{-1}. Upon the reduction to the mono- (**3**−**6**) and dianions (**1** and **2**),

(24) Hush, N. S. *Prog. Inorg. Chem.* **1967**, *8*, 357.

(25) (a)Attia, A. S.; Pierpont, C. G. *Inorg. Chem.* **1997**, *36*, 6184. (b) Jung, O.-S.; Jo, D. W.; Lee, Y.-A.; Chae, H. K.; Sohn, Y. S. *Bull. Chem. Soc. Jpn.* **1996**, *69*, 2211.

(26) The observed $\chi_m T$ for **1** is by 20% larger than those of **2**, for example, $\chi_m T$ = 1.49 (350 K), 1.46 (300 K), 1.30 (100 K), and 0.65 (2 K) emu·K·mol^{-1}. The deviation from the curve estimated for **2** (ground state is $S = 1$) could not be accounted for by the single-crystal structure and spectroscopic data of **1**. To reproduce the observed data, the species with higher than $S = 1$ spin should be introduced. The used sample for the measurement was microcrystalline powder, therefore unexpected paramagnetic impurity could be one reason for the deviation. The obtained data is deposited just for the Supporting Information.

(27) Lynch, M. W.; Buchanan, R. M.; Pierpont, C. G.; Hendrickson, D. N. *Inorg. Chem.* **1981**, *20*, 1038.

(28) Gordon, D. J.; Fenske, R. F. *Inorg. Chem.* **1982**, *21*, 2907.

Table 5. Solution (CH_2Cl_2) and Solid State (KBr) Absorption Spectral Parameters for $Cr^{III}(X_4SQ)_3 \cdot 4C_6H_6$ (X = Cl and Br) and **1**−**6**

compound	ν_{max} ($10^3 \times cm^{-1}$) ($\epsilon_{max} = 10^3 \times M^{-1} \cdot cm^{-1}$)									
					Solution/CH_2Cl_2					
$Cr(Cl_4SQ)_3$			8.70 (sh, 8.87)	10.0 (1.39)		13.0 (4.85)			19.0 (20.8)	22.0 (sh, 8.96)
$Cr(Br_4SQ)_3$			8.13 (sh, 10.4)	10.0 (1.35)		12.8 (6.70)			18.5 (26.9)	21.6 (sh 9.60)
1	5.94 (3.38)		8.30 (sh, 1.23)			12.7 (2.88)	14.7 (2.00)		18.5 (3.95)	22.0 (2.86)
2	6.04 (4.66)		8.30 (sh, 1.51)			12.7 (4.24)	14.5 (3.38)		18.5 (5.40)	21.9 (4.43)
3	4.55 (5.23)				11.4 (sh, 4.18)	12.4 (5.12)	14.9 (7.13)	16.0 (sh, 6.72)	18.2 (7.50)	21.6 (5.11)
4	4.59 (5.06)				11.4 (sh, 4.12)	12.4 (5.08)	14.9 (7.00)	15.9 (7.02)	18.3 (8.03)	21.5 (5.46)
5	4.55 (5.95)				11.4 (sh, 5.37)	12.3 (6.63)	14.7 (8.69)	15.7 (8.48)	18.3 (10.7)	21.3 (6.78)
6	4.59 (5.93)				11.4 (sh, 6.06)	12.9 (9.19)	14.8 (9.96)	16.0 (9.87)	18.9 (24.4)	22.0 (sh, 13.6)
					Solid/KBr					
$Cr(Cl_4SQ)_3$			7.81	9.35		12.7			18.3	
$Cr(Br_4SQ)_3$			7.94	9.80		12.9			18.2	
1	5.56		8.00 (sh)			12.0	14.6		18.2	21.5
2	5.62		8.33			12.1	14.5		18.5	21.3
3[a]	3.92	5.88 (sh)	8.70 (sh)		10.8 (sh)	12.1	14.3		17.7	21.1
4	4.36	5.88 (sh)	8.70 (sh)		11.2 (sh)	12.0	14.0	15.9 (sh)	17.4	21.1
5	4.35	5.26 (sh)	8.70 (sh)		10.9 (sh)	11.8	14.0	15.6	17.4	21.1
6	3.85	5.88 (sh)	8.33 (sh)		10.9 (sh)	12.3	14.5	15.0 (sh)	18.0	21.1 (sh)

[a] Reference 5.

Table 6. The IVCT Band Shape Data and Estimated Hush Coupling Energy, H_{ab}, for **1**−**6** in CH_2Cl_2 at 296 K

compound	λ_{max} (nm)	ν_{max} (cm^{-1})	ϵ ($M^{-1} \cdot cm^{-1}$)	$\Delta\nu_{1/2}$ (cm^{-1})[a]	$r = d_{OO}$ (Å)[b]	H_{ab} (cm^{-1})
1	1690	5940	3380	2410	2.76	1630
2	1660	6040	4660	2110	2.683	1860
3	2200	4550	5230	2910	2.71[c]	1990
4	2180	4590	5060	2830	2.709	1940
5	2200	4550	5950	2740	2.6	2150
6	2180	4590	5930	2740	2.641	2120

[a] Half-widths of bands are calculated from the higher $\nu_{1/2}$ assuming symmetric bands. [b] The shortest O···O distances obtained from crystallographic data are taken as r_{OO}. [c] Reference 5.

the bands appear near 4500 (**4**−**6**) and 6000 (**1** and **2**) cm^{-1}. These bands are assigned to intervalence charge transfer (IVCT) bands of SQ ← Cat,[2b] indicating the presence of both forms of the ligand in the $[Cr^{III}(X_4SQ)_{3-n}(X_4Cat)_n]^{n-}$ ($n = 2$ (**1** and **2**) and 1 (**4**−**6**)) anions. The band shape data are summarized in Table 5. From the spectra we can estimated the degree of electric coupling, H_{ab}, using the well-known Hush formula[24] for mixed-valence complexes given in eq 1,

$$H_{ab} = (2.05 \times 10^{-2})[\epsilon_{max}\Delta\nu_{1/2}/\nu_{max}]^{1/2}\nu_{max}/r_{OO} \qquad (1)$$

where ϵ_{max} is the maximum extinction coefficient of the absorption band in $M^{-1} \cdot cm^{-1}$, $\Delta\nu_{1/2}$ is the bandwidth at half ϵ_{max}, ν_{max} is the energy of the absorption in cm^{-1}, and r_{OO} is the distance between donor and acceptor wave functions. Using the values of r_{OO} (shortest distances between oxygen atoms) listed in Table 6, H_{ab} are evaluated. The calculated values are three times greater than that of cobalt complexes,[2a] indicating strong coupling interaction between SQ and Cat through the chromium ion.

In conclusion, the absorption spectra clearly detect the species in different oxidation states and the spectra of redissolved samples show that even in the solution the species exist just as well as in the solid states.

Electronic Absorption Spectra of Solid. Figure 10 shows absorption spectra of complex $Cr^{III}(Cl_4SQ)_3 \cdot 4C_6H_6$, **1**, **4**, and **6** in the solid state (KBr pellets). The observed spectral parameters are listed in Table 5. In both regions A and B, the maximum of each peak for all the compounds tends to shift to lower energy than that of solution. In region B, compounds **1** and **2** show broad, intense bands at 5560 and 5620 cm^{-1}, respectively, while those of **3**−**6** are found in the region 3850−4360 cm^{-1} (Figure 10b). As well as the solution spectra, the absorption band is assigned to IVCT (SQ ← Cat) transition, indicating the presence of both forms of the ligand. The peak maxima are comparable to those for manganese (4760 cm^{-1})[25a] and cobalt (4170 cm^{-1})[25b] complexes containing 3,5-di-*tert*-butyl-*o*-semiquinonate and catecholate. The isostructural compounds **3** and **4** show identical spectral patterns, reflecting the similarity of electronic structures. Compound **5** having a bromo derivative also shows a spectrum with the IVCT band at 4350 cm^{-1} as well as those of previously reported three 1:1 CT compounds containing $[Co^{III}Cp_2]^+$ (4350 cm^{-1}), $[TMTSF]^+$ (4080 cm^{-1}), and $[TMTTF]^+$ (4170 cm^{-1}).[5]

Temperature Dependence of Magnetic Susceptibilities. The temperature dependence of the molar magnetic susceptibility of **2**−**6** and $Cr^{III}(Cl_4SQ)_3 \cdot 4C_6H_6$ is shown in Figure 11 as plots of $\chi_m T$ vs T. For compound **2**, at 350 K, $\chi_m T$ is equal to 1.26 $cm^3 \cdot K \cdot mol^{-1}$, which is higher than 1.00 $cm^3 \cdot K \cdot mol^{-1}$ ($g = 2.00$) of $S = 1$ spin expected for antiferromagnetically coupled $S = {}^3/_2$ (Cr^{III}) and ${}^1/_2$ (SQ) spins, while much lower than 2.25 $cm^3 \cdot K \cdot mol^{-1}$ ($g = 2.00$) for two non-interacting spins.[26] As the temperature is lowered, the value gradually decreases to reach 0.684 $cm^3 \cdot K \cdot mol^{-1}$ at 2 K. The profile of this curve indicates that the Cr^{III}−SQ interaction is strongly antiferromagnetic, leading to a $S = 1$ ground state and a $S = 2$ excited state for the molecule. The exchange interaction (J) between the chromium ion and the SQ was estimated with a simple dimeric model with eq 2,

$$\chi_M = \frac{N\mu_B{}^2 g^2}{k(T-\Theta)} \frac{2 + 10e^{4x}}{3 + 5e^{4x}} \qquad (2)$$

where $x = J/kT$ and N, g, μ_B, k, and Θ mean Avogadro's number, isotropic g-factor, Bohr magneton, Boltzmann constant, and Curie−Weiss constant to the gauge intermolecular interac-

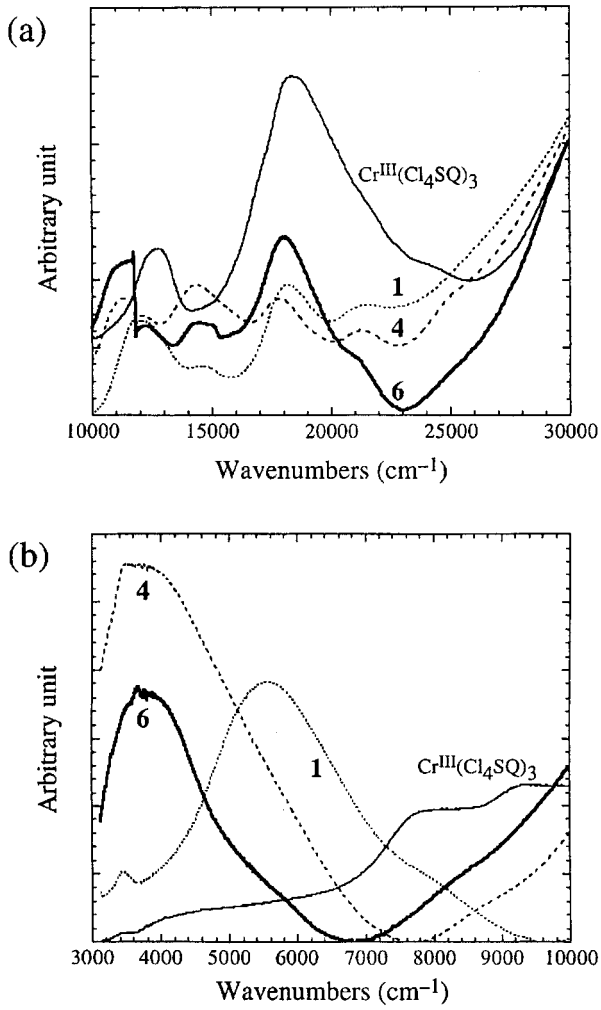

Figure 10. Electronic absorption spectra of **1** (···), **4** (---), **6** (—), and $Cr^{III}(Cl_4SQ)_3 \cdot 4C_6H_6$ (−) in the solid state (KBr). The spectrum of **2** is similar to that of **1**, while those of **3** and **5** are similar to that of **4** (see Supporting Information).

tions. The best fit to eq 2 gives $g = 2.02$, $J = -170$ cm^{-1}, and $\Theta = -0.9$ K. The obtained J value is smaller than -400 and -350 cm^{-1} estimated for $Cr^{III}(Cl_4SQ)_3$ and $Cr^{III}(phenSQ)_3$, respectively.[27] The intramolecular antifferomagnetic interaction in **2** is weaker than those of monoanionic species, $[Cr^{III}(X_4SQ)_2(X_4Cat)]^-$ (vide infra), which show only a small amount of thermal population to the exited state ($S = {}^3/_2$), even at 350 K. The relatively weak intramolecular magnetic interaction of **2** is associated with the large energy separation of magnetic orbitals of the chromium ion and the ligands compared with those of $[Cr^{III}(X_4SQ)_2(X_4Cat)]^-$.[28] Together with this effect, the strong electron-withdrawing substituent on X_4SQ could promote the decreasing of antiferromagnetic interaction in the molecules.[3(b)] In contrast, the χ_mT value of **3** at 350 K is 0.430 emu·K·mol^{-1}, which is close to the theoretical value of 0.375 emu·K·mol^{-1} expected for $S = {}^1/_2$ ($g = 2.00$). Therefore, the unpaired electron is consistent with strong antiferromagnetic interactions between the $S = {}^3/_2$ (Cr^{III}) and two $S = {}^1/_2$ spins on the SQ ligands.[29]

At 350 K, χ_mT values of **4** and **5** containing paramagnetic $[Fe^{III}Cp_2]^+$ ($S = {}^1/_2$) are 1.29 and 1.33 cm^3·K·mol^{-1}, respectively. The values are larger than the sum of spins on the $[Fe^{III}Cp_2]^+$ ($S = {}^1/_2$) and $[Cr^{III}(Cl_4SQ)_2(Cl_4Cat)]^-$ ($S = {}^1/_2$), due

(29) Wheeler, D. E.; McCusker, J. K. *Inorg. Chem.* **1998**, *37*, 2296.

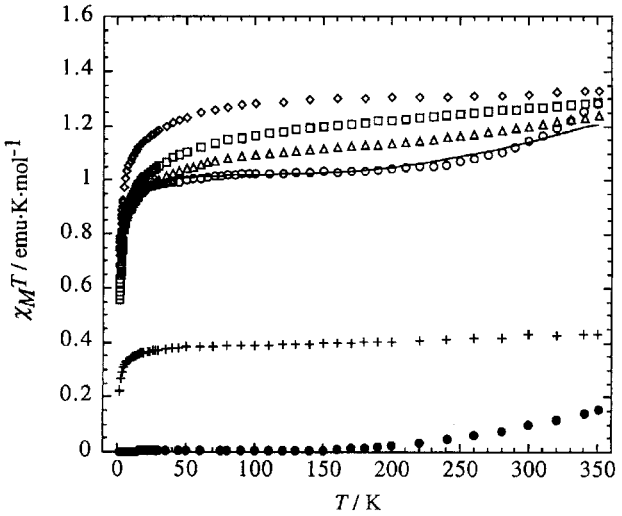

Figure 11. Temperature dependence of χ_mT plots of **2** (○), **3** (+), **4** (□), **5** (◇), **6** (△), and $Cr^{III}(Cl_4SQ)_3 \cdot 4C_6H_6$ (●). The solid line corresponds to the fit of the experimental data to a dimeric model (see text).

to significant orbital contributions of $[Fe^{III}Cp_2]^+$ to χ_mT values over the spin only value of 0.75 cm^3·K·mol^{-1}.[30] These values show weak temperature dependencies in the 30−350 K region and decrease rapidly under 30 K. The decreasing of χ_mT in the lower temperature region suggests the presence of zero-field splitting effect and/or intermolecular antiferromagnetic interactions between the neighboring paramagnetic centers. The interactions result from close packings of neighboring molecules in the column as found in the X-ray structure analyses. Furthermore, these are attributable to the intermolecular X···X contacts between the adjacent anionic complexes (Table 4). In the case of **4**, the presence of the direct stacking structure between the $[Fe^{III}Cp_2]^+$ and the $[Cr^{III}(Cl_4SQ)_2(Cl_4Cat)]^-$ causes the magnetic interactions between them.[30]

For compound **6**, χ_mT is equal to 1.24 cm^3·K·mol^{-1} at 350 K and, as the temperature is lowered to 200 K, gradually decreases to reach a value of 1.14 cm^3·K·mol^{-1}. Finally, the value decreases rapidly until 0.757 cm^3·K·mol^{-1} at 1.9 K, followed by another decrease to 60 K. Figure 11 shows also the temperature-dependent magnetic susceptibility for $Cr^{III}(Cl_4SQ)_3 \cdot 4C_6H_6$ in the same temperature region. At 350 K, the compound has χ_mT value of 0.154 emu·K·mol^{-1}, which drops to a value of 0.002 emu·K·mol^{-1} at 1.9 K. As reported previously,[3b] the complex has a ground state of $S = 0$ as a result of strong intramolecular antiferromagnetic interaction between three unpaired electrons of Cr^{III} and three SQ ligands. Actually, χ_mT value shows temperature dependency associated with Boltzmann distribution from the $S = 0$ ground state to the $S = 1$ exited state. At 350 K, the $S = 1$ excited state is weakly populated. The subtraction of this contribution from that of **6** provides a temperature dependence of the χ_mT curve similar to those of **4** and **5**. The magnetic data can be accounted for by the presence of the two chromium complexes, $[Cr^{III}(Cl_4SQ)_2(Cl_4Cat)]^-$ and $[Cr^{III}(Cl_4SQ)_3]^0$, as well as FT-IR spectrum.

Conclusions

The CT reactions of $Cr^{III}(X_4SQ)_3$ (X = Cl and Br) with $M^{II}Cp_2$ (M = Co and Fe) give 2:1, 1:1, and 1:2 donor−acceptor CT compounds. During the reactions, $Cr^{III}(X_4SQ)_3$ com-

(30) Miller, J. S.; Calabrese, J. C.; Rommelman, H.; Chittipeddi, S. R.; Zhang, J. H.; Reiff, W. M.; Epstein, A. J. *J. Am. Chem. Soc.* **1987**, *109*, 769.

plexes are reduced to $[Cr^{III}(X_4SQ)_2(X_4Cat)]^-$ and $[Cr^{III}(X_4SQ)(X_4Cat)_2]^{2-}$. The dianionic form can be obtained only by use of two equivalent $Co^{II}Cp_2$, and is first structurally and spectroscopically characterized in the solid state. Both anionic forms contain the SQ and Cat, showing the bands in the region 3130−10000 cm^{-1}, characteristic of IVCT transition between the two ligands. The crystal structures of CT compounds are dependent on the charge of the anions; the $[Cr^{III}(X_4SQ)(X_4Cat)_2]^{2-}$ in **1** and **2** show discrete molecular structures, while the $[Cr^{III}(X_4SQ)_2(X_4Cat)]^-$ in **4**−**6** form one-dimensional column structures, which are constructed from the two sets of ligand stacking interactions of chromium complexes. The remaining ligands interacted with $[Fe^{III}Cp_2]^+$ and C_6H_6 in **3** and **4** to form additional one-dimensional ···[D][A][S][D][A]··· type mixed-stack arrangements. On the other hand, compound **6** forms a two-dimensional sheet structure where the two redox isomers $[Cr^{III}(Cl_4SQ)_2(Cl_4Cat)]^-$ and $[Cr^{III}(Cl_4SQ)_3]^0$ are included. Therefore, the compound is regarded as a mixed-valence molecular assembly. Interestingly, this mixed-valence state of the chromium module is dependent on the redox active nature of the coordinated ligand.

Acknowledgment. The authors acknowledge financial support by a Grant-in-Aid for Scientific Research (Priority Area No. 10149101) from The Ministry of Education, Science, Sports and Culture of Japan.

Supporting Information Available: Crystal and structure refinement data, positional parameters, anisotropic displacement parameters, and complete listings of bond distances and angles of **1**, **2**, and **4**−**6**, in CIF format. The crystal packing structures of **4**−**6**, the absorption spectra of **2**, **3**, and **5**, and temperature dependence of $\chi_m T$ for **1**. This material is available free of charge via the Internet at http://pubs.acs.org.

IC0003832